RESEARCH PAPER

Biopolymer-biocement composite treatment for stabilisation of soil against both current and wave erosion

Anant Aishwarya Dubey[1,2] · Jack Hooper-Lewis[2] · K. Ravi[1] · Navdeep Kaur Dhami[2] ·
Abhijit Mukherjee[2]

Abstract

Increased frequency of extreme weather events has made the conservation of riverbanks and coastlines a global concern. Soil stabilisation via microbially induced calcite precipitation (MICP) is one of the most eco-suitable candidates for improving resilience against erosion. In this study, the erosion characteristics of soil treated with various levels of biocementation are investigated. The samples were subjected to hydraulic flow in both tangential and perpendicular directions in a flume to simulate riverbank and coastal situations. Soil mass loss, eroded volume, and cumulative erosion rates of the treated soil against the applied hydraulic energy density have been reported. Post erosion exposure, the residual soil has been assessed for its properties using needle penetration resistance, precipitated calcium carbonate content and microstructure. It was observed that soil erosion declined exponentially with the increase in calcium carbonate content against the perpendicular waves. However, biocementation leads to brittle fracture beyond a threshold, limiting its efficacy, especially against the tangential waves. Additional composite treatment with a biopolymer was found to improve the resilience of the soil specimens against erosion. The composite treatment required half of the quantity of the biocementing reagents in comparison to the equally erosion-resistant plain biocemented sample. Therefore, stoichiometrically the composite treatment is likely to yield 50% lesser ammonia than plain biocement treatment. This investigation unravels a promising soil conservation technique via the composite effect of biocement and biopolymer.

Keywords Biocementation · Biopolymers · Coastal erosion · Microbial induced calcite precipitation (MICP) · Riverbank erosion

1 Introduction

Natural soil erosion of coasts and riverbanks is a complex phenomenon that occurs with the interaction of current, waves, tides and wind [61]. Soil erosion occurs due to several factors such as internal hydraulic pressure (internal erosion), current as experienced in riverbanks (current erosion) as well as waves as in seacoasts (wave erosion). Generally, they have been studied separately. To simulate coastal conditions, laboratory tests have been performed in hydraulic flumes by estimating soil erosion against perpendicular waves [27, 32, 55]. In the case of riverbank erosion, bridge scours, and earth-filled embankment dams, a tangential current without waves has been employed [13, 26, 62]. In reality, a complex interaction of current and wave erosion is experienced. When the waves hit the coastline at an oblique angle, nearshore wave breaking produces shore parallel current [2], while in the riverbanks, the shallow waves coexist with tangential current [14]. Therefore, it is crucial to consider both forms of erosion for its successful mitigation.

Present soil erosion control measures such as sea walls, concrete revetments, geomembranes/geotextiles, sandbags filters and artificial reefs are based on the principle of attenuating the hydraulic waves and arresting the eroding materials, which are aesthetically disagreeable, expensive and non-durable [13, 41, 60]. Alternate erosion prevention

✉ Abhijit Mukherjee
   abhijit.mukherjee@curtin.edu.au

1 Department of Civil Engineering, Indian Institute of
   Technology, Guwahati 781039, India

2 School of Civil and Mechanical Engineering, Curtin
   University, Kent St., Perth, WA 6102, Australia

techniques by means of improving the soil resilience utilising the synthetic chemical grouts are hazardous for the geo-environment and aquatic life [15, 40]. In Nature, on the other hand, a plethora of natural aggregation of sand is observed in the form of beach rocks [19]. Figure 1 illustrates a freestanding natural beach rock at Eagle-bay, Rottenest Island of Western Australia, withstanding erosion forces. Ramachandran et al., 2020 [49] have unravelled the biogenic and abiogenic biocementation processes responsible for such formations and emulated them in the laboratory. Although there are many pathways to biocementation, a calcite precipitation approach via the urea hydrolysis pathway, also known as microbially induced calcite precipitation (MICP), has found popularity in laboratory simulations due to their ease of control, durability and rapid soil strength improvement [36, 46, 57]. Applications of MICP for soil improvement have been explored in strength enhancement [1, 11, 28, 45], aeolian erosion control [17, 23], internal erosion control [38], tidal current-induced erosion control [51], rainfall-induced erosion control [12, 39], tangential flow-induced erosion control [13, 26, 62] and immobilisation of toxic metals [30, 54, 65].

The authors are unaware of any prior study on the performance of biocemented sand against erosion caused by the hydraulic waves in conjunction with the current. There are only a handful of reports on biocementation mediated erosion mitigation against hydraulic waves. Shahin et al., 2020 [53] reported less than 5% erosion with a calcite content of 1.52% against erosional wave action for two hours. Kou et al., 2020 [41] reported minimum soil erosion occurred to a sample with 30.1% calcite content within the investigated range of MICP treatment against the hydraulic waves in a 30-min test. On the other hand, Liu et al., 2021 [44] reported that two cycles of MICP treatment were inefficient to prevent erosion for a 2-h test duration without quantifying the precipitated calcite content. Behzadipour and Sadrekarimi, 2021 [7] reported that negligible erosion occurred to a physical riverbank model treated with 20 cycles of biochar-assisted biocementation treatment against 600 strong waves. It is evident from these studies that the number of cycles of biocementation treatment, i.e., the quantity of $CaCO_3$ precipitates, is one of the deciding factors to control erosion. Moreover, these studies have reported the erosion characteristics against the wave features such as dimension, frequency and test duration. For upscaling the laboratory results to the field, a study correlating the erosion traits of the biocemented soil against wave energy is imperative.

Usually, a consistent decrease in soil erodibility is reported with the increase in biocementation levels. Salifu et al. [51] have reported that a 53° soil slope filled up with 9.9% of soil pores with $CaCO_3$ effectively endured 30 tidal cycles without a notable erosion. In our previous studies on

Fig. 1 Natural beach rocks against the destructive wave at Eagle Bay, Rottenest Island, Australia (Photograph taken by the author)

current erosion [25, 26], the potential of indigenous strains of the Brahmaputra river to mitigate soil erosion at various slopes against the tangential hydraulic current has been reported. It was observed that against a fluvial current ranging from 0.06 to 0.62 m/s, a sample with calcite content of around 7% resulted in a fourfold reduction of the weight of eroded soil in comparison to the untreated soil. However, brittle chunks of aggregated sand were also observed at heavy biocementation. Similar observations were made in previous researches [13, 21]. A combination of biopolymer treatment along with standard biocementation has been reported to alleviate the brittle fracture of biocemented soil against the tangentially flowing hydraulic current [26]. However, the proposed bio-composite material has not been tested against hydraulic waves.

From the above discussion, it is evident that although there is anecdotal evidence of biocementation in mitigating soil erosion, several gaps are yet to be filled. Although there are separate studies for current and wave erosion, in practice they occur simultaneously. The present study evaluates biocemented soil against both current and wave loads. Two sets of experiments with perpendicular waves and the tangential waves in conjunction with current have been conducted. For scaling the experimental results up to field conditions, the excitation parameters must be quantified in a judicious way. In this investigation, the cumulative erosion rates of different levels of biocemented sand slopes have been plotted against the total wave energy density. The plots are of much importance for achieving soil stabilisation for a specific field condition. In addition, the level of stabilisation of the soil has been estimated through a needle penetration test that can be applied in the field. A correlation curve has been drawn between the calcium carbonate content and the penetration resistance value. The curve will assist the field engineers to estimate the amount of cementation for achieving a corresponding strength. Moreover, the biopolymer-biocement composite has been compared with the standard biocementation for its efficacy to prevent wave-induced erosion. The average erosion rates are correlated with Needle Penetration Index (NPI) within the viewpoint of potential field application. Extensive microstructural analysis has been conducted to investigate the mechanism of soil binding with different kinds of bio-stabilisation techniques.

2 Materials and methods

2.1 Soil

Fine natural sand was procured from Cook Mineral Industries, Perth, Western Australia. The grain size distribution equivalent to the riverbanks and coasts was selected based on the previous reports [25, 53]. The evaluated engineering properties of the soil as per the American society of testing materials (ASTM) protocols are illustrated in Table 1. The soil is characterised as poorly graded fine sand (SP), as per the unified soil classification system (USCS).

2.2 Microbe and biopolymer

For biocementation purposes, a ureolytic bacteria (BS3) isolated from loose sand of a riverbank site in one of our previous studies [25] was utilised for biocementation purposes in this study. The isolated strain exhibited around 98% similarity in their genomic sequence with *Sporosarcina pasteurii* (ATCC 11,859). The indigenous biocementing soil bacteria are reported to be dominating in the long run over the foreign biocementing microbe *Sporosarcina pasteurii* [18, 31]. The bacteria were grown in the yeast extract-ammonium sulphate (YE) media. The growth media consisted of yeast extract (20 g/l), tris buffer (0.13 M), and ammonium sulphate (10 g/l). Each constituent of the media was autoclaved separately before mixing. The initial pH was adjusted to 8.5 by adding a few drops of 5 N NaOH solution to cementation media prior to autoclaving. The organisms were cultivated overnight to the exponential phase, and the growth was monitored with its optical density at 600 nm ($O.D._{600}$). The specific urease activity of the microbe was evaluated as 6.44 mM urea hydrolysed per minute per unit $O.D._{600}$ by the electrical conductivity method [64].

Table 1 Geotechnical properties of the soil utilised in this study

Properties	Values	Reference protocols
D_{60} (mm)	0.25	ASTM D6913 [5]
D_{30} (mm)	0.2	
D_{10} (mm)	0.15	
Coefficient of uniformity (C_u)	1.67	
Coefficient of curvature (C_c)	1.06	
USCS classification	SP	
Maximum dry unit weight (kN/m³)	17.65	ASTM D4254-16 [3]
Minimum dry unit weight (kN/m³)	15.5	
Specific gravity, (Gs)	2.6	ASTM D854-14 [6]
Shape, Texture	Angular, smooth	SEM
Minerals	Quartz, Mica	XRD
pH	7.3	ASTM D4972-19 [4]

The hydrophilic polysaccharide biopolymer xanthan gum was also used in this study. Xanthan gum is yielded as a metabolic by-product from the microbial community *Xanthomonas campestris*. The analytical grade of the biopolymer powder was procured from Sigma-Aldrich. The biopolymer solution was prepared by mixing the xanthan gum powder at a low concentration of 1 g/l in hot water (around 80° C) with a magnetic stirrer [24, 26].

2.3 Soil sample preparation and experimental summary

The soil samples were prepared in two distinct configurations to simulate tangential and perpendicular waves against the soil specimen similar to the river and coastal waves. For the perpendicular waves test (P), the samples are prepared in an acrylic mould of dimension 100 mm width, 100 mm length, and 100 mm depth, maintaining a 45° slope (1 horizontal to 1 vertical). For tangential waves tests (T), the soil samples were prepared in a container of dimension 92.5 mm length, 58 mm width, and 40 mm depth. Later, the container was plugged in an acrylic slope of 45 degrees (1 horizontal to 1 vertical). The acrylic slope was gradually sealed along the walls of the flume with a smooth ramp to cause minimum interference to the flow. It must be noted that initial volume was different for both the tests as it required different kinds of setup/arrangements in the hydraulic flume to simulate the tangential and perpendicular wave. Only the surface of the soil specimens was exposed to flow for erosion in both scenarios. All the tests are conducted on triplicate samples, and the average values of results along with deviations have been reported.

For preparing the soil specimens, a three-step biocementation approach was adopted with the aim of uniform precipitation [22, 34]. The sand was washed with ultrapure water, dried, and sterilised before the sample preparation to avoid the possibility of abiogenic precipitation by the contaminants. The sand specimens were poured at a dry density of 1.56 Mg/m^3 for both cases. After pouring the sand, at the first step, one pore volume of the fixation solution containing 25 mM of calcium chloride ($CaCl_2$) was sprayed. At the second step, one pore volume of the cultivated bacteria at $O.D._{600}$ value equivalent to 1 was sprayed on the dried specimen, and samples were retained for 24 h. Later at the third stage, one pore volume of the cementation solution was sprayed. The cementation media consisted of 0.5 M urea, 0.5 M $CaCl_2$, and 1 g/l of yeast extract. These three steps are considered to comprise one MICP treatment cycle (M1). The samples were dried for 24 h at 35 degrees Celsius in a fan-equipped oven after completion of each step. Following the discussed MICP treatment protocol, soil specimens with multiple cycles were prepared (M2-M8). The intended tests and

experimental summary are demonstrated in Fig. 2. The untreated samples have been mentioned as control (M0). Additionally, to prepare biopolymer-biocement composites (XM), soil samples were prepared by spraying xanthan gum solution as pre-treatment to MICP [26]. The samples were prepared by single spraying of one pore volume of 1 g/l xanthan gum solution on the dry sand. The plain biopolymer treated specimen is termed XM0. Later, MICP treatments with intended levels were performed, and the samples prepared are termed XM2 and XM4.

Each of the biocemented samples has been tested for tangential as well as perpendicular waves. Triplicates of the set of eight different types of soil samples were prepared, including the above-mentioned control sample (M0), four different levels of biocementation (M2-M8) and three combinations of biopolymer aided biocementation (XM0-XM4) for each case. The samples subjected to tangential waves are labelled with a prefix T with the treatment nomenclature in the form of TM0, TM2-TM8, and TXM0-TXM4. With a similar approach, the samples subjected to the perpendicular waves are labelled with suffix P, namely PM0, PM2-PM8, and PXM0-PXM4. After, the flume erosion tests, needle penetration resistance, calcium carbonate content, and the microstructure of the treated soil samples have been evaluated.

2.4 Wave simulation in the hydraulic flume erosion tests

The different configurations are presented in Fig. 3. Both the scenarios were simulated in a 12 m Armfield tilting flume with the glass-walled channel of flow cross-section of 300 mm width and 320 mm height. The maximum test duration (30 min) was considered based on the trials on the cohesionless soil, which was heavily eroded as soon as the waves hit the specimens.

The plan and cross-section for the test configuration to simulate the perpendicular hydraulic waves are illustrated in Fig. 3a and c. The waves were modelled based on the actual waves at Rottenest Island [53]. The waves are generated on still water at depth (h) 50 ± 5 mm in the hydraulic flume scaled at 1:250. The generated waves were set to propagate at wave height (h_w) of 28 mm and wavelength (λ) of 1500 mm with a 0.33 Hz frequency (f). To ensure the generation of shallow surging erosional waves, three parameters were maintained, 1. $h > h_w/0.6$; 2. $h < \lambda/20$; and 3. $h_w < \lambda/7$ [29, 53].

To simulate tangential waves, the alignment of the soil specimen is kept tangential with the flow to let the wave strike the soil in the intended tangential direction, as illustrated in Fig. 3b and d. A gentle flow velocity was maintained at 0.06 m/s throughout the test with a constant water depth (h) of 50 ± 5 mm. The hydraulic current is
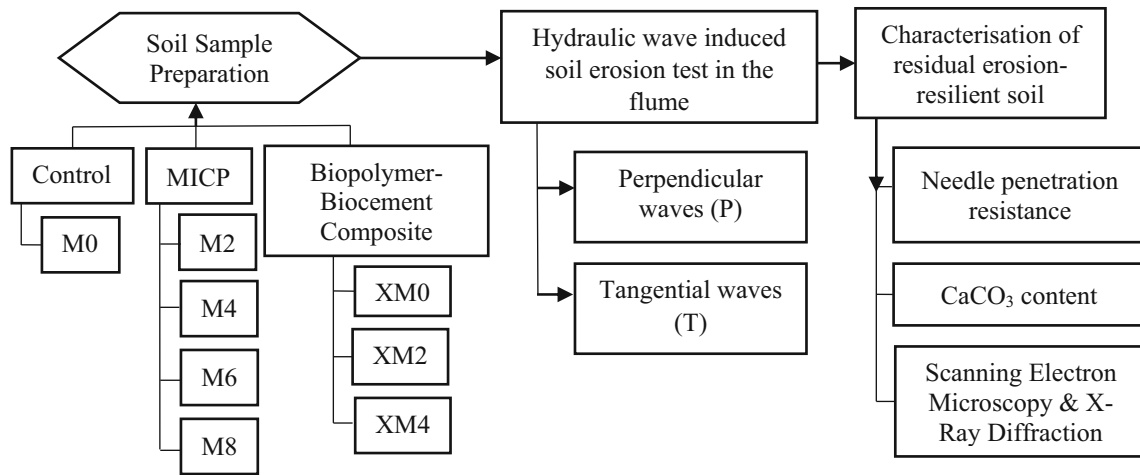
Fig. 2 Summary of experiments
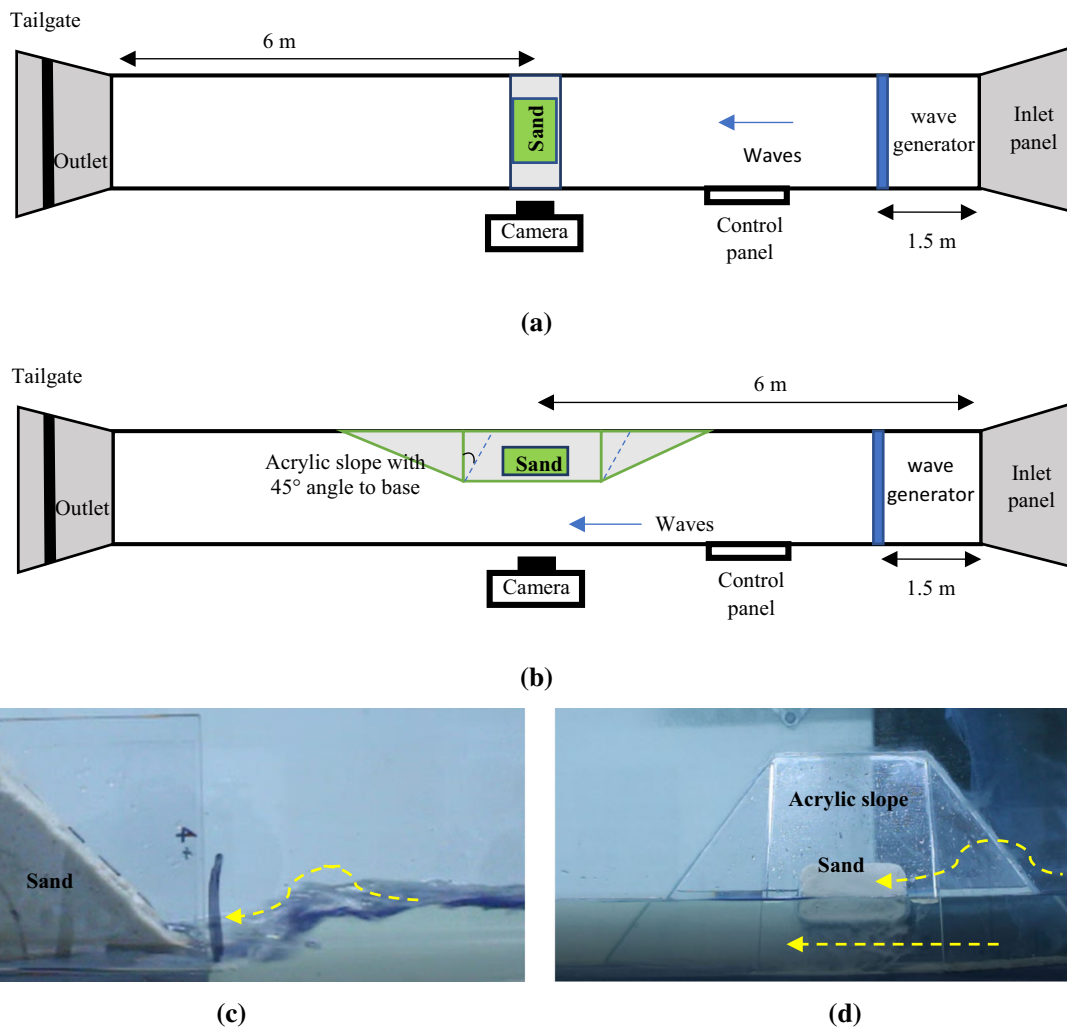

(a)

(b)

(c)

(d)

Fig. 3 Schematics of the top view of configurations for **a** perpendicular wave test, and **b** tangential wave test; and corresponding front view photograph in (**c**) and (**d**)

kept much slower than the theoretical, critical velocity (V_c) to negate the hydraulic current-induced soil erosion, which is calculated as 0.175 m/s from Briaud's equation [8]. The waves were produced utilising a pedal type of wave generator placed at 1.5 m from the inlet. The generated waves were set to propagate at wave height (h_w) of 25 mm and wavelength (λ) of 1500 mm with a 0.33 Hz frequency. These parameters were adopted to mimic shallow wave conditions of the natural environment in the hydraulic flume fulfilling the three criteria of 1. (λ/h) in the range of 1 to 25; 2. (λ/h_w) in the range of 4 to 56, and 3. (kh) < ($\pi/100$) as recommended by few of the previous studies [14], where k is the wavenumber.

The erosion was recorded with a Digital Single-Lens Reflex (DSLR) camera for image analysis. The cumulative erosion rate (E_R) is defined as the total volume eroded within a time interval. The cumulative erosion rates are presented against the total applied wave energy density (E_D), which is evaluated from Eqs. 1 and 2.

$$E = \frac{\rho g h_w^2}{8} \tag{1}$$

$$E_D = \int_0^t \frac{E.f.}{A_S} dt \tag{2}$$

where E is the wave energy as per linear shallow water wave theory, ρ is the density of the water, g is gravitational acceleration, h_w is the wave height, f is the frequency of waves, and A_s is the exposed surface area of the soil [56]. The parameter E_D (Joules/cm^2) is derived from Eq. 1 to normalise the total energy impacting per unit area (cm^2) of the soil.

The stills of the recordings were used to evaluate the total volume eroded in the percentage of the initial volume (V) at different time intervals with the open-source software ImageJ. The eroded volume (V) of the sample at a particular E_D was calculated by following Eq. (3).

$$V = \frac{V_i - V_t}{V_i} \times 100 \tag{3}$$

where V_i is the initial volume of treated specimen and V_t is the volume of retained soil at time 't' responding to the particular E_D.

For comparison of the efficiency of biocementation levels to improve the erosion resilience, the soil mass loss (m_L) is also compared. The soil mass loss (%) is calculated after drying the residual sample following Eq. (4).

$$m_L = \frac{m_i - m_r}{m_i} \times 100 \tag{4}$$

where m_i is the initial mass of treated soil and m_r is the mass of the residual soil.

2.5 Needle penetration resistance, CaCO$_3$ content, and microstructure analysis

Post-flume erosion experiments, the strength of the residual biocemented crust was evaluated by conducting the needle penetration test on at least five distinct points of each sample. The International Society of Rock Mechanics (ISRM) recommended the needle penetration test for quick evaluation of weakly cemented soil and soft rocks [20, 58, 59]. The ratio of needle penetration resistance (N) to the penetrated depth (mm) is defined as the needle penetration index (NPI). The needle penetration tests were conducted at the penetration rate of 15 mm/min on a universal testing machine (Shimadzu AGS-X) equipped with Chenile needle #22, having a diameter of 0.86 mm.

After the penetration, the dried sample was scraped out in triplicates from 5 mm beneath the penetration points. The sample was washed with ultrapure water to remove the free calcium ions. Then, the soil was dried, and 5 g soil was collected. The collected soil (5 g) was washed with 25 ml of 2 N HCl [12]. The precipitated calcium carbonate (CaCO$_3$) content (mg/g -soil) was measured based on the difference in weight of the dry weight of retained soil on Whatman filter grade #1 after the acid washing and the dry weight of soil sample collected after washing (5 g). The carbonate content of the untreated sand was also measured to consider the possibility of abiogenic carbonate content.

The soil was collected from the biocemented crust for microstructure analysis. The microstructure of all the biocemented soil was first visualised with a portable handhold digital optical microscope at low magnifications. After the confirmation of soil bonding, scanning electron microscopy (SEM) was conducted to visualise the calcium carbonate bridging in the treated soil samples on Tescan Vega 3 instrument. For SEM imaging, the air-dried soil specimens were affixed on the aluminium stub and coated with a 10 nm platinum coating. The mineralogical analysis of the precipitates, the X-ray diffraction (XRD) analysis was conducted on Bruker D8 advanced diffractometer with Nickel filtered Cu-Kα radiation varying 2θ from 5° to 90° with a step size of 0.013°.

3 Results and discussion

3.1 Flume erosion test

3.1.1 Performance of biocemented soil

Figure 4a shows the percentages of soil volume eroded (V) with the increasing energy density of the perpendicular waves (E_D). The corresponding cumulative erosion rates
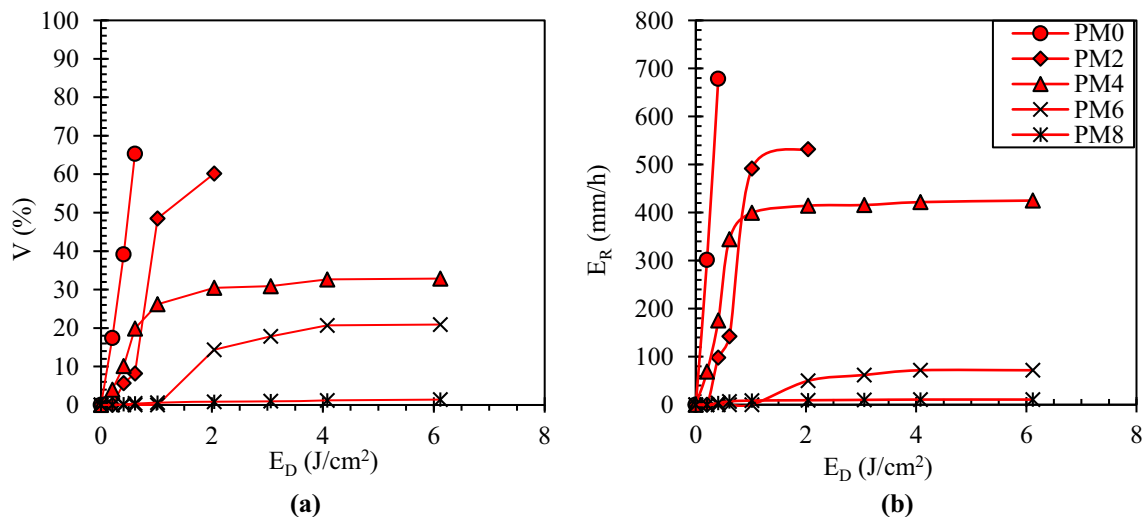
Fig. 4 Comparison of **a** percentage volume eroded and **b** cumulative erosion rates for different levels of the biocemented soil against perpendicular waves

(E_R) is shown in Fig. 4b. The graphs are plotted until either 65% of the volume is eroded or the maximum wave energy is reached. The threshold E_D is defined as the wave energy density at which soil erosion initiates.

The biocement treatment prevents erosion till the wave energy reaches to threshold E_D. Once the threshold E_D is reached, soil erodes rapidly. Eventually, the soil loss plateaus and the biocemented specimen takes a shape that minimises the impact of waves. Another possible reason for plateauing might be that the weakly biocemented grains at the top surface got eroded first as they were continuously disturbed due to the multiple spraying of treatment solutions. Therefore, the soil volume loss and cumulative erosion rates exhibit the S shape curve for most of the specimens against the applied wave energy.

The untreated sample PM0 lost 65% of mass at a low E_D (0.6 J/cm^2). Thus, unstabilised sand has a high rate of cumulative erosion, as shown in Fig. 4b. The rate of erosion reduced substantially with biocementation. The threshold E_D goes higher with increasing cementation. For the same E_D (0.6 J/cm^2), PM2, treated with the lowest level of biocementation, had only 8% erosion. Thus, even with a relatively low biocementation, erosion from a moderate E_D can be mitigated. However, with increasing E_D, the sample experienced an increasing rate of erosion. Finally, it lost 65% of its volume at E_D 2 J/cm^2. Thus, it is clear that higher levels of cementation would be required as wave energy increases. In comparison, PM4 lost only 32% of its volume when the maximum E_D around 6 J/cm^2 was reached. PM6 exhibited a maximum of 21% V with a much-reduced E_R value of 71 mm/h. PM8 exhibited negligible erosion.

The V and E_R values against E_D for the tangential waves are plotted in Fig. 5a and b. Although the nature of the curves was similar to that of the perpendicular waves, there are significant differences. TM0 lost more than 65% of its volume at a low E_D of 1 J/cm^2. TM0 displayed a high cumulative erosion rate around 338 mm/h. At the same E_D, the eroded volume of samples TM2, TM4, TM6, and TM8 were observed as 38.9, 37.5, 30, and 19%, respectively. Thus, biocementation is effective against the tangential flow as well. However, in this experiment, tangential waves caused a higher level of erosion than the perpendicular waves for the corresponding level of wave energy. This is due to the drag force exerted on the sample by the tangential wave. This force creates shear stress on the samples, which tends to dislodge their upper crust.

TM4 was significantly more erosion resistant than TM2. TM6 and TM8 endured the maximum designed E_D of 5.3 J/cm^2. The total eroded volume for TM6 was observed to be 46% at the maximum E_D. Interestingly, TM8 lost 9% more volume than TM6 despite having the highest level of biocementation treatment. Previous studies [13, 21] have also reported that the samples may become brittle after a threshold level of cementation is crossed. This aspect is investigated in the next section by visually comparing the samples.

Photographs of biocemented samples post erosion exposure are presented in Fig. 6a–h. With the introduction of biocementation, the aggregation of sand particles can be easily identified in Fig. 6f. PM2 and TM2 were identified with the lightly biocemented sand (LBS) aggregates. At this stage, although aggregation was observed on the surface of the specimens, it is not uniformly distributed. With the increasing number of treatments, a biocemented crust
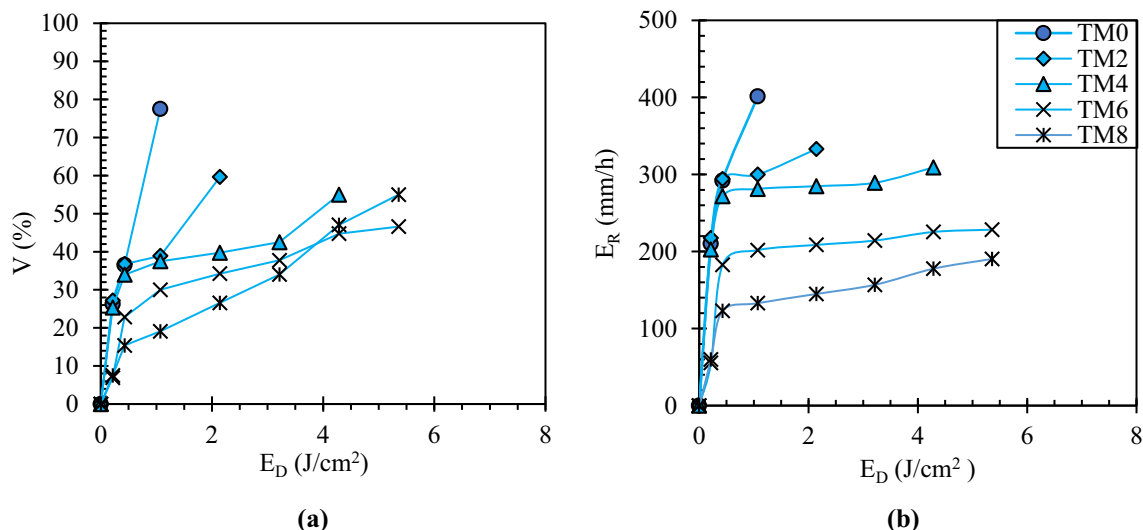
Fig. 5 Comparison of **a** percentage volume eroded and **b** cumulative erosion rates for different levels of the biocemented soil against tangential waves
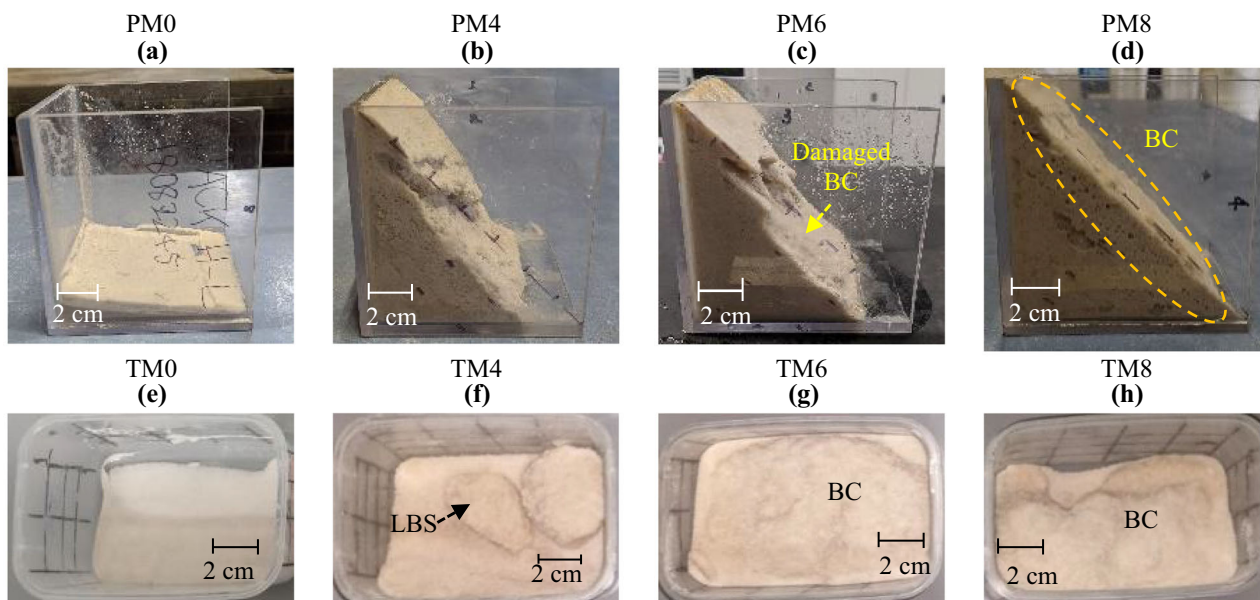

Fig. 6 Biocemented soil samples post-erosion exposure against **a–d** perpendicular and **e–h** tangential waves

(BC) was observed. TM4 was observed to have a relatively thin BC, which was dislodged by the higher energy tangential waves. With visual observation on the images of residual samples, it was noticed that the thickness of biocemented crust increased. The increased crust thickness in PM4 and PM6 protected them from erosion to a great extent despite getting subjected to much higher E_D. Contrary to TM4, the dislodgement of deteriorated BC did not occur in PM4 and PM6, possibly due to the distinct nature of the impacting perpendicular waves. The perpendicular waves break upon hitting the soil, producing uprush and backwash currents. The uprush current detaches the weak

soil grains, and the backwash current transports the detached grains with the induced drag [37]. On the other hand, in the case of tangential flow, the waves flowing over the fluvial current induce additional shear on the bank material [14], resulting in severe soil erosion. The eroded material is immediately transported by the tangential current. PM8 exhibited negligible erosion confirming that in the case of perpendicular waves, the soil erosion decreased consistently with the increase in biocementation. Contrarily, TM8 was observed to be more weathered than TM6. Brittle chunks of the cracked biocemented layers from
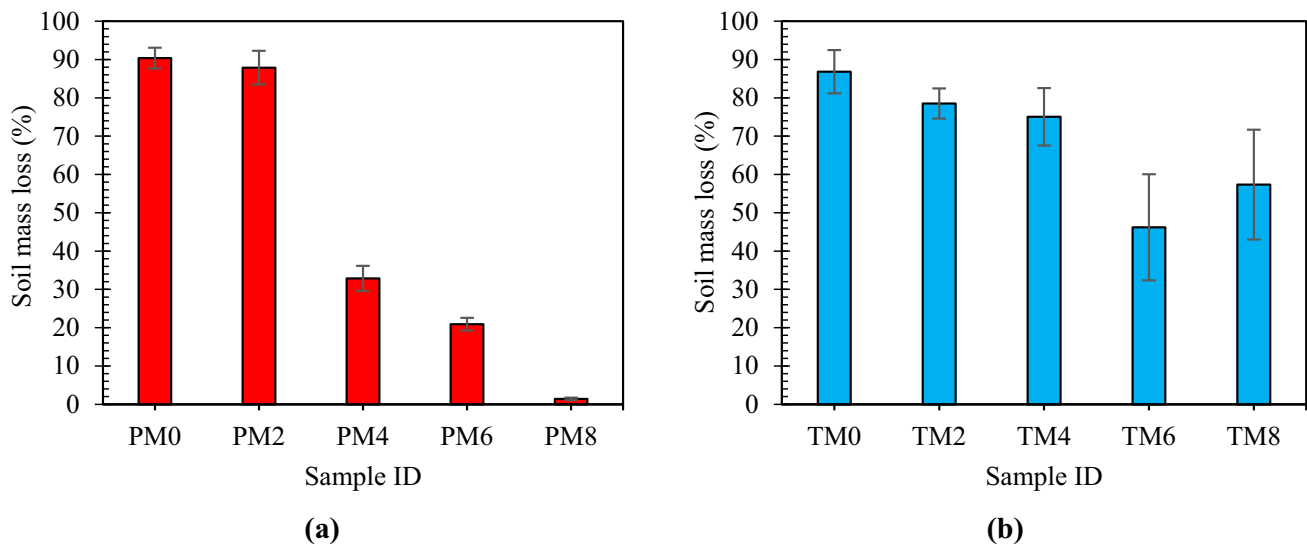
Fig. 7 Comparison of soil mass loss with the various biocemented soil against **a** perpendicular and **b** tangential waves

TM6 and TM8 were observed to be drawn away with the tangential flow.

The soil mass loss post-erosion exposure is reported in Fig. 7a and b. The protection against soil loss improved with the increase in biocementation levels. PM0 and PM2 demonstrated a massive soil mass loss of around 90%. However, it is to be recalled from Fig. 4a that the required wave energy to erode the equivalent amount of soil was notably higher for PM2 than PM0. Thus, although light biocementation is effective for moderate waves, higher levels of treatment would be necessary against high wave energy. The soil mass loss receded with the increase in biocementation levels. PM4 and PM6 lost only 32% and 20% of soil mass loss. Soil erosion against the perpendicular waves was negligible (1.4%) after eight cementation cycles.

In the case of tangential waves, the soil mass loss for TM0 was recorded around 90%, same as PM0. However, the rest of the samples exhibited different responses against erosion. The soil mass loss for TM2 and TM4 was observed around 75%. Minimum soil mass loss was recorded for TM6 as 46% as the soil was protected with a thick biocemented crust, as illustrated in Fig. 6g. TM8 exhibited a mass loss of 57%, more than TM6. The increase in soil mass loss in TM8 indicates that an increase in biocementation levels does not essentially lead to improvement in the erosion resilience of the soil in case of the tangential flow.

In previous studies on hydraulic wave-induced erosion, the erosion characteristic of the biocemented samples is reported in terms of soil mass loss and decline in the slope angle of the bank against the duration and number of erosional waves. Shahin et al. [53] exposed biocemented sand to erosional waves of height 6.9 cm and wavelength 23 cm for two hours and reported less than 5% soil mass loss with a calcite content of 1.52%. Kou et al., 2020 [41] have reported that the minimum soil erosion in terms of decline in slope angle at various slopes (10°, 20° and 35°) with a sample containing 30.1% calcite content in the residual soil against the hydraulic wave amplitude around 4 cm and frequency of 1 cycle per minute for a 30-min test. On the other hand, Liu et al., 2021 [44] compared MICP with EICP (enzyme induced calcite precipitation) treated calcareous sand (98% carbonate) and reported that for a 2-h duration of wave action of the height of 0.4 cm and 0.8 cm with a frequency of 2.2 Hz, both the treatments were inefficient to prevent long-term erosion on steep slopes. Both MICP and EICP samples were treated soils with two cycles of cementation solutions failed when exposed to the hydraulic waves for a longer duration. However, the calcite content was not quantified in the study. The inefficiency of the MICP and EICP to prevent erosion might be due to low $CaCO_3$ precipitation. In the present study, the samples treated with low levels of biocementation (M2) also failed at a relatively low wave energy impact. Behzadipour and Sadrekarimi, 2021 [7] have employed biochar-assisted biocementation for erosion mitigation on a physical model of riverbank slope of Karoon river, Iran, against wave-action and demonstrated that a heavily biocemented sample treated with 20 cycles of cementation solution remained largely stable against the impact of 600 strong waves of height 7 cm and frequency two cycles per second. The features of waves such as wave dimension, frequency and test duration were different in the aforementioned studies, which is most likely the reason for the differences in the findings. This study is the first to report the erosion

characteristics against the cumulative wave energy density, which could be a more practical parameter for designing the required levels of biocementation for erosion mitigation at the field. However, a field-scale trial is necessitated to verify the applicability of the proposed experimental findings.

3.1.2 Performance of biopolymer-biocement composite

The erosion characteristics of samples that received a biopolymer pre-treatment (XM) have been reported in Figs. 8 and 9, along with the dotted lines denoting results with no such pre-treatment. In this case too, the experiments were also halted either in case of 65% of the volume was lost or once the maximum wave energy was achieved. The curves followed a similar S pattern as in the case of MICP treated specimens. However, the XM treatment (continuous lines) was observed to be more resistant to soil erosion than the plain MICP treatment treated with equivalent biocementation reagents.

Figure 8a and b illustrates the erosion behaviour of the XM treated specimens against the perpendicular waves in terms of V (%) and E_R (mm/h) against E_D (J/cm^2). It was observed that the sample treated only with the biopolymer (PXM0) resisted erosion better than PM0. PXM0 lost 57.5% of its initial volume, with a high E_R of 489 mm/h at the E_D value of 2 J/cm^2. With the introduction of MICP treatment to the biopolymerised specimen, the erosion reduced substantially. PXM2 and PXM4 endured the maximum wave energy. Plateauing of erosion curves of PXM2 and PXM4 was also observed in this case; however, PXM2 and PXM4 were observed to outperform their counterparts PM2 and PM4. PXM4 exhibited a fourfold reduction in the eroded volume in comparison with PXM2.

PXM4 eroded only 11% of the total volume at the maximum E_D value of 6 J/cm^2. The corresponding E_R values reduced from 229 to 30 mm/h while comparing PXM2 and PXM4. The erosion resilience of heavily biocemented sample PM8 was found to be comparable with the biopolymer aided moderately biocemented PXM4. It is to be noted that plain biopolymer stabilised (0.5% of soil weight) poorly-graded sand without any fine content has been reported to lose its strength after interaction with moisture [48].

The erosion characteristics of the XM specimens against the tangential waves are reported in Fig. 9a and b. TXM0 was eroded around 65% of its volume at a low E_D of 1 J/cm^2, similar to the untreated sample TM0, indicating that mere low-viscosity biopolymer treatment might not be enough to prevent soil erosion against high-energy tangential waves. Conversely, the soil treated with biopolymer aided biocement exhibited considerably high erosion resistance. The erosion resistance of TXM2 and TXM4 surpassed the best performing conventionally biocemented samples TM6 and TM8. TXM4 exhibited a more than threefold reduction in erosion in terms of the total volume eroded when compared to TXM2. The maximum V for TXM4 was observed as 16.75% at the maximum E_D. These observations clearly demonstrate the efficacy of biopolymer pre-treatment before MICP.

Figures 10a–h are photographs of the samples before and after the erosion test. It is evident that biopolymer pre-treatment has prevented fragmentation, as observed in MICP samples. The biopolymer-biocement crust (BBC) is clearly more resilient than the biocement crust (BC). PXM2 was damaged somewhat at high-energy waves (Fig. 10c). Comparatively, TXM2 provided appreciable protection against the erosion induced by the tangential
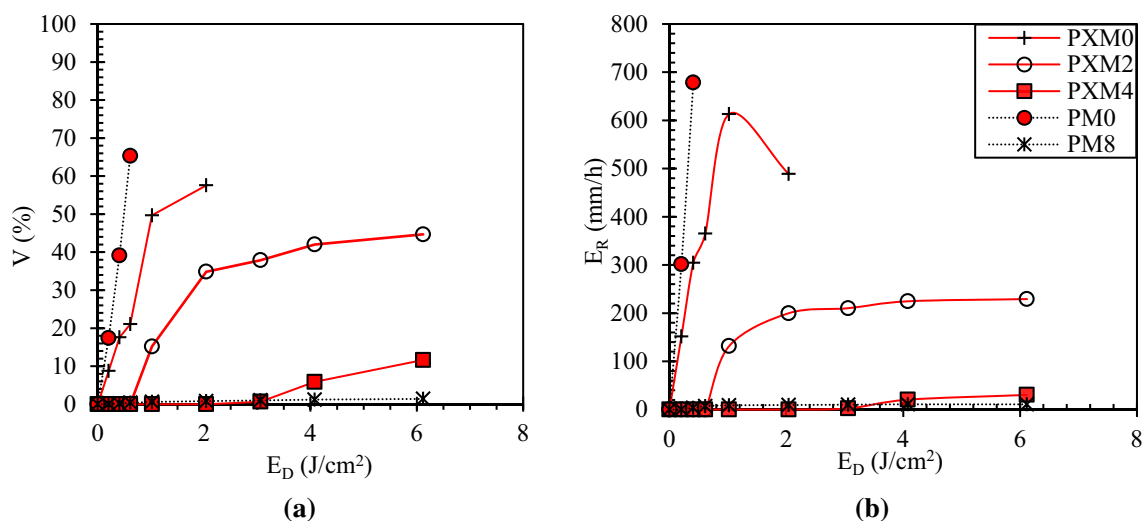

Fig. 8 Comparison of **a** percentage volume eroded and **b** cumulative erosion rates for different levels of XM treated soil samples against perpendicular waves
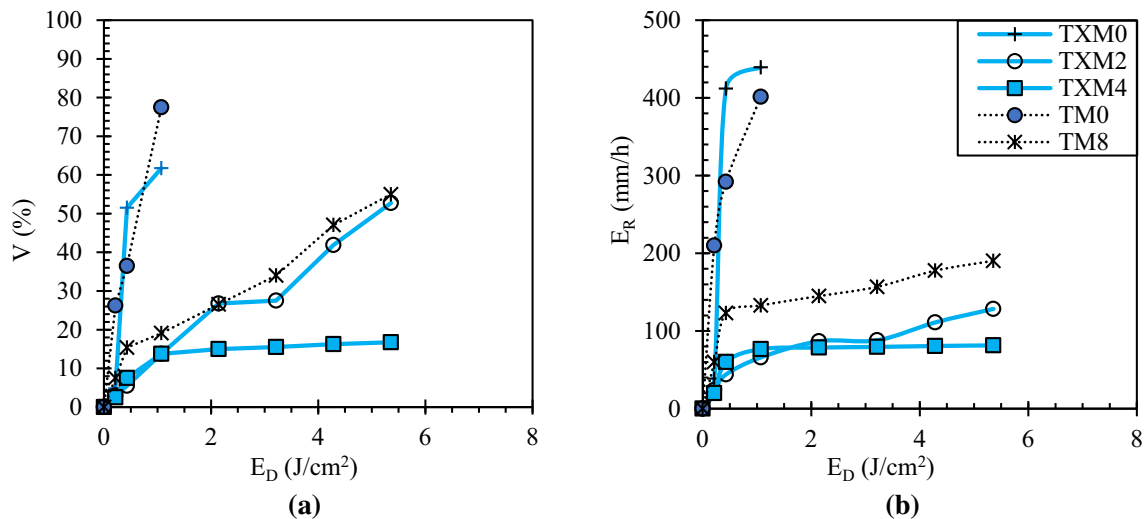
Fig. 9 Comparison of **a** percentage volume eroded and **b** cumulative erosion rates for different levels of XM treated soil samples against tangential waves
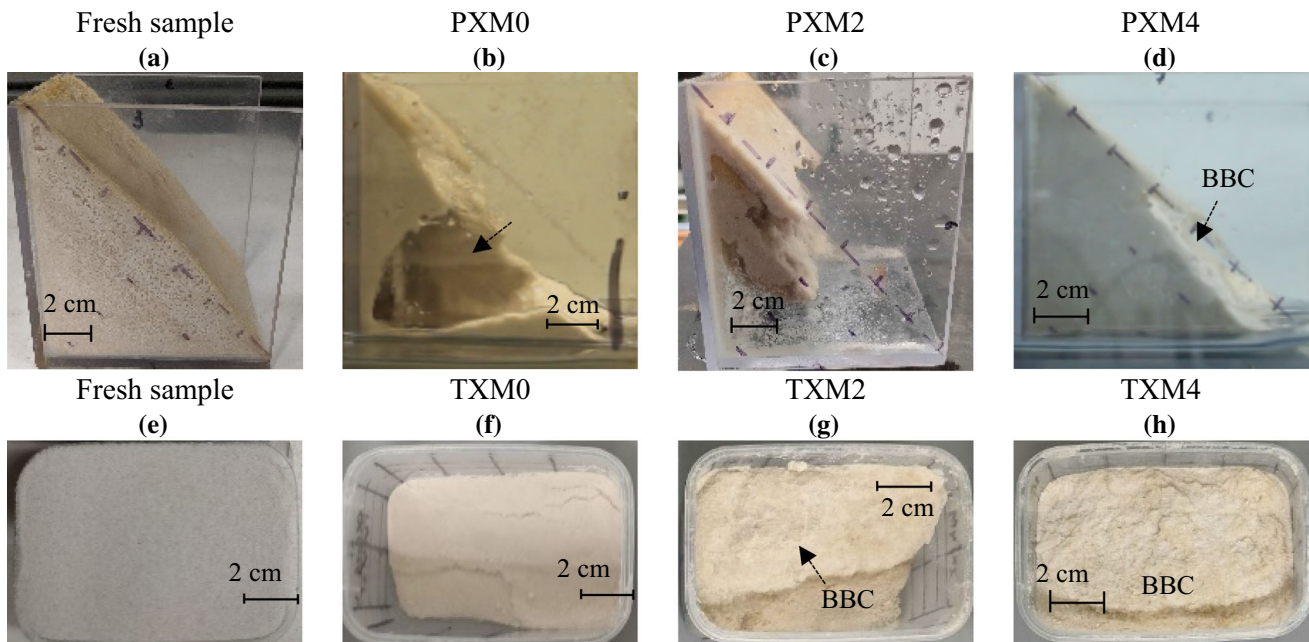

Fig. 10 Biopolymer-biocement composite samples post erosion exposure against **a–d** perpendicular and **e–h** tangential waves

waves. A thick protective BBC was observed for TXM4 and PXM4 samples, which resulted in marginal soil loss against the eroding waves.

A visual comparison between biopolymer-biocement composite treated specimens TXM4 and plain biocemented specimens TM4 from Figs. 10 (h) and 6(f) indicates that comparatively, a more uniform distribution of carbonates happened in the biopolymer-biocement composite treated specimens, which led to the development of a biocemented crust. On the other hand, the plain biocemented specimens TM4 only exhibit aggregation of sand due to

biocementation. It is to be noted that Wang et al. 2018 [62] have considered making the cementation solution in poly-vinyl alcohol (PVA) for controlling the location of pre-cipitation to the intended depth. In this study, instead of modifying the cementation reagent, the soil was supple-mented with one pore volume of low viscosity biopolymer solution (Xanthan Gum) prior to biocementation for the same purpose. However, further investigations are required to find the best approach to control the uniformity of $CaCO_3$ precipitation. Different biopolymers at varying viscosities must be investigated to determine the best

suitable combinations for the biopolymer-biocement composite. Continuous application of low concentration bio-cementation reagents along with bacterial solution employing irrigation like micro-sprinkler spraying system is suggested for future studies. The continuous micro-sprinkler spraying systems are often used in irrigation [66] to supply the water uniformly to the field, which might also be suitable for a field-scale MICP application.

The performance of the XM treated specimens in terms of soil mass loss is reported in Fig. 11. The soil mass loss observed for PX, PXM2, and PXM4 were 76, 62 and 24%, whereas the observed soil mass loss for TXM0, TXM2, and TXM4 were 83, 45, and 21%. From Fig. 11, it is evident that with the XM treated soil samples, the erosion resilience improved consistently with the increase in MICP levels. It may be recalled that with MICP treatment alone, brittle behaviour was observed in the case of relatively high level of biocementation. Such behaviour was avoided with biopolymer pre-treatment.

Apart from the enhanced erosion resistance, there are several other benefits of using the biopolymer as an aid to conventional biocementation. Application of biopolymer would be helpful to substantially reduce the required materials' quantity, associated cost and environmental impact of the conventional biocementation. The bio-composite material has been reported to produce 36% less ammonia for an equally efficient erosion-resistant biocemented specimen against the hydraulic current varying from 0.06 to 0.62 m/s [26]. In this study, we observed that stoichiometrically, only half of the biocementation reagents would be required for the best performing XM treated specimen (PXM4) in comparison to the best performing MICP treated specimen (PM8) with similar performance for erosion control. Theoretically, it will also reduce the generation of harmful by-product ammonia by 50%, making the proposed biopolymer aided biocementation (XM) treatment a preferred alternative over the conventional MICP. In the case of tangential waves, 33.33% lesser chemical reagents would be required for preparing TXM4, considering TM6 the best performing soil specimen. Interestingly, a threefold erosion resilient material will be produced with TXM4 in comparison with TM6, considering the total volume eroded (V).

3.2 Needle penetration index and CaCO₃ content

The needle penetration index (NPI) values of the residual samples are presented in Fig. 12a and b. As the samples for both sets were treated with the same methodology, a comparable NPI for the counterparts were expected. The NPI values for samples prepared for perpendicular setup (PM2-PM8) varied from 9 N/mm to 21 N/mm, respectively. The NPI values for samples prepared for tangential setup (TM2-TM8) were found in a range of 5.5 to 21 N/mm, respectively. A notable difference was observed only in TM2 and PM2, which could be possibly due to the use of residual samples that have undergone different wave actions. XM treated specimens displayed NPI in a similar range to the equivalent biocemented specimens. Negligible NPI values were recorded for TXM0 and PXM0, indicating that the biopolymer in the present concentration does not contribute to improving the stiffness of the soil. PXM2 and PXM4 exhibited NPI values of 10.58 and 15.38 N/mm. Whereas the NPI values for TXM2 and TXM4 were evaluated as 10.3 and 14.63 N/mm. It is well known that the polymer has a considerably lower elastic modulus in comparison to either sand or biocement. Thus, it does not add significantly to the penetration resistance.
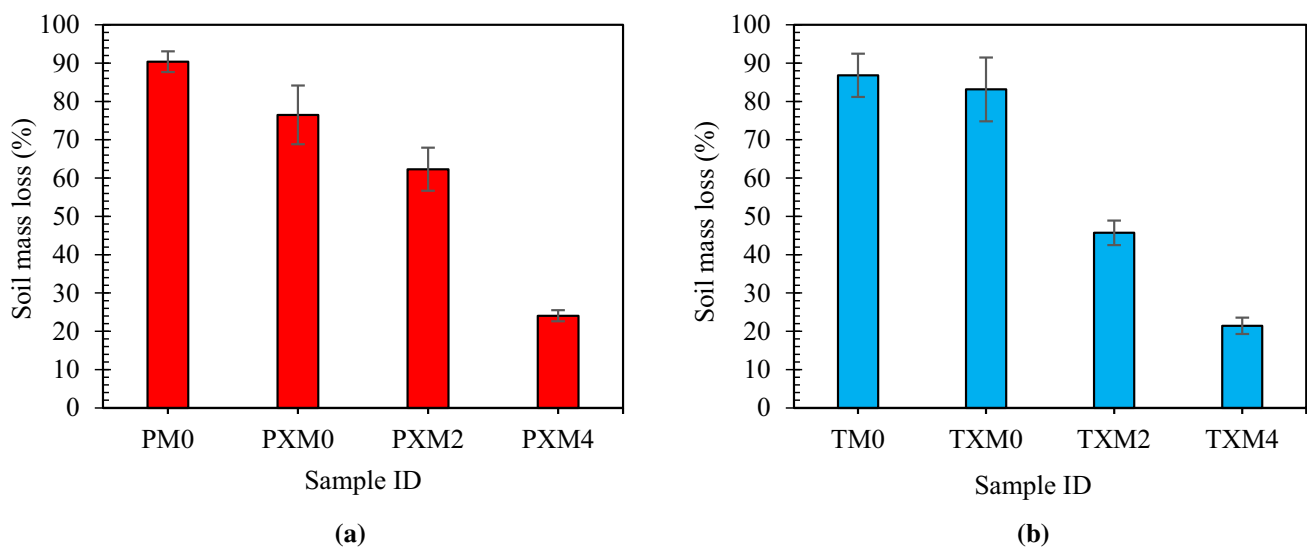

(a)

(b)

Fig. 11 Comparison of soil mass loss with the various biopolymer-biocement composite soil against **a** perpendicular and **b** tangential waves
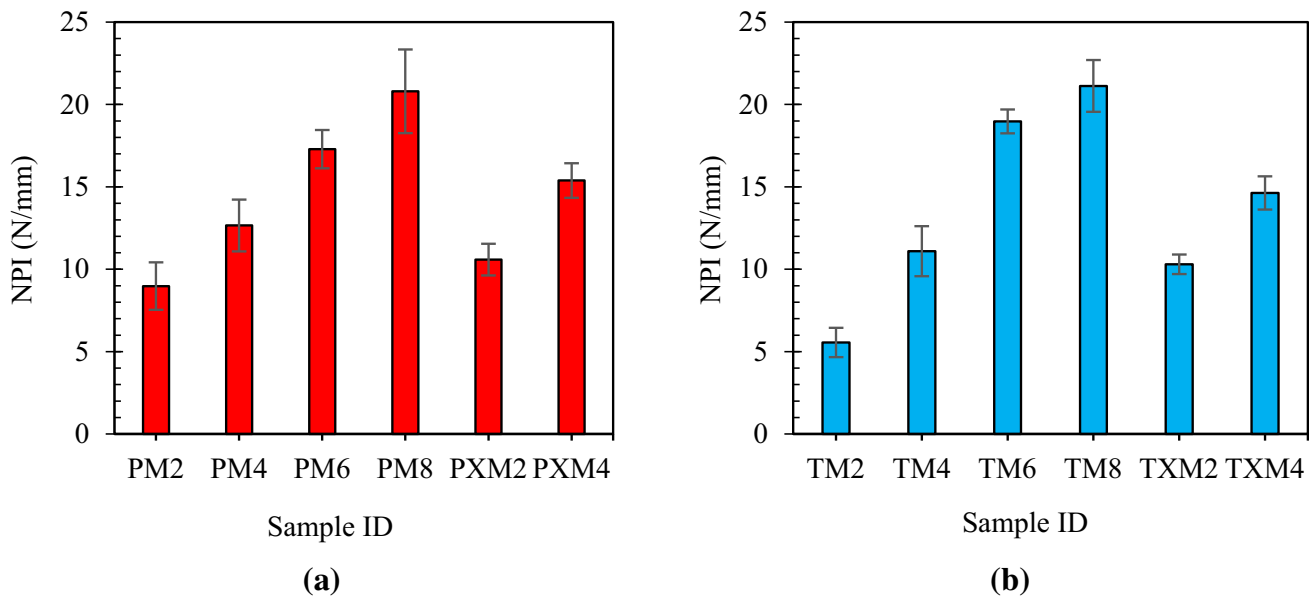
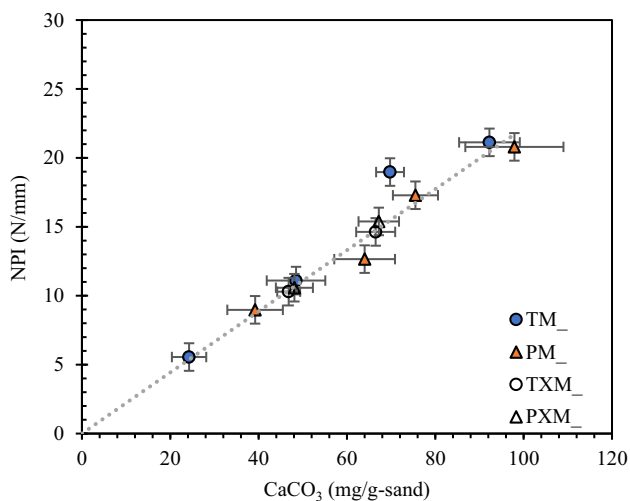**Fig. 12** Needle penetration index (NPI) of the treated soil samples

Fig. 13 Correlation of needle penetration index (NPI) with $CaCO_3$ content

A correlation between $CaCO_3$ and NPI is attempted. The $CaCO_3$ content of the soil at the penetration points was evaluated and plotted against the NPI values, as illustrated in Fig. 13. The average $CaCO_3$ content for residual PM2, PM4, PM6 and PM8 was found to be 38, 64, 76 and 98 mg/g of sand, respectively. While in the case of residual TM2, TM4, TM6 and TM8, the $CaCO_3$ was found to be 24, 48, 70 and 93 mg/g-sand, respectively. The average $CaCO_3$ contents were found to be consistent with NPI values. The biopolymer-biocement composite treated specimens PXM2, TXM2, PXM4 and TXM4 were found to be 47, 48, 66 and 67 mg $CaCO_3$ content per g of sand.

The average $CaCO_3$ and NPI measurements after the treatment are vital for investigating the efficiency of treatments. However, it was not determined in the current study. It is to be noted that a multiple bacterial recharge strategy was adopted in the current study, and the fresh bacteria were added to soil after each biocementation cycle to maintain the maximum precipitation rates in lieu of the prior studies [42, 47]. Lai et al. 2021 [42] reported almost 100% calcium conversion efficiency with the repeated injection of bacteria per treatment below 1 Molar concentration of cementation solution. Murugan et al. 2021 [47] reported that the kinetic constant of calcium carbonate precipitation could be maintained with additional recharge of bacteria. Stoichiometrically, one biocementation cycle (M1) adds 12.5 mg $CaCO_3$ per gram of sand. The residual samples were investigated post-erosion exposure for their average $CaCO_3$ content and NPI, considering that they have sustained the wave energy up to a particular level in the test configurations. This will help to design the MICP treatment for a target $CaCO_3$ content and NPI against the known wave energy for a large-scale application. The average $CaCO_3$ contents of the residual samples are found to be higher than the theoretical $CaCO_3$ as the weaker biocemented grains were eroded during the wave action. Therefore, it must be considered as a limitation of the current study.

Despite the restrictions of the described experimental conditions and materials used in the study, a good agreement ($R^2 > 0.9$) was observed between C and NPI values with a linear relationship as shown in Eq. (5).

$$NPI = 0.22(C) \qquad (5)$$

Here NPI is the needle penetration index in N/mm and C is the average CaCO$_3$ content in mg/g-sand. In Fig. 13, TM_ and PM_ denotes the results from different levels of the residual biocemented samples from tangential and perpendicular waves erosion experiments. The TXM_ and PXM_ are the results obtained from the residual soils of the XM treated specimens at various levels against tangential and perpendicular waves erosion experiments. It may be noted that these correlations are valid for the present experimental conditions only. The average NPI is observed to be linearly dependent on the average precipitated CaCO$_3$ content in the considered range of 0 to 100 mg/g-sand in the current study. The proposed equation may vary with the type of soil, type of microbes and quality of CaCO$_3$.

NPI can be a convenient method of assessing biocementation in the field. Chung et al. 2021 [12] have reported a consistent increase in the NPI values with a similar needle penetration equipment from Maruto Co. Ltd., ranging from 9.6 N/mm to 21.1 N/mm for the calcite content up to 85 mg/g-sand in the fine-to-medium grained sand. The present study is the first attempt to develop a relationship between the two parameters. Further research on the correlation of NPI with different calcite content and soil strength are recommended for different kinds of soil. It is also to be noted that the acid washing protocol may overestimate the CaCO$_3$ content due to the presence of residual ammonium chloride, undissolved urea-CaCl$_2$, and non-carbonate substances [10]. To avoid the overestimation of CaCO$_3$, the samples were washed in ultrapure water prior to acid washing.
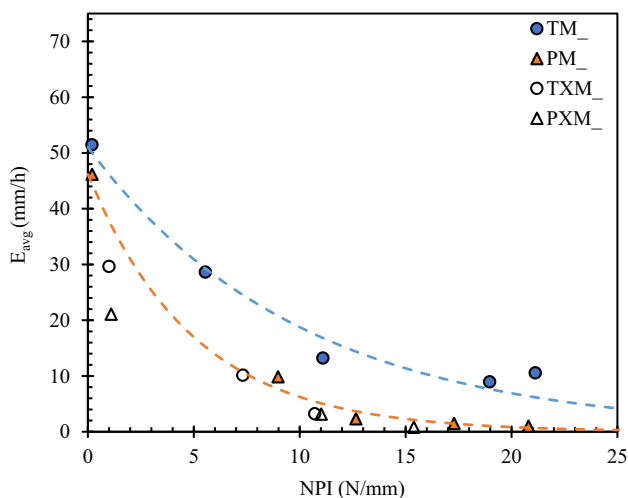
3.3 Correlation of average erosion rate with NPI

The average erosion rate (mm/h) with respect to the average NPI values of the treated soils are presented in Fig. 14. The average erosion rate (mm/h) is defined as total volume eroded (V$_e$) during the experimental duration (T) per unit surface area (A$_s$) of the specimen, as shown in Eq. 6.

$$E_{avg} = \frac{V_e}{A_s \times T} \tag{6}$$

With vegetation-based bank protection against surficial erosion, several researchers have correlated the erosion rate in exponentially declining models considering several controlling parameters such as vegetation cover (%), root length and root density [67]. In a recent study, the soil erosion rate is reported to decline exponentially with root density against the hydraulic wave-like impact [52]. Adopting a similar model, the average erosion rates (E$_{avg}$) and the NPI values are correlated in Eq. 7.

$$E_{avg} = A.e^{-B.(NPI)} \tag{7}$$

Here A (mm/h) and B (mm/N) are the fitting parameters. A is set as the maximum erosion rate for the untreated soil. While the fitted parameter B, which derives the decline rate of the erosion curve, is dependent on material strength properties as well as the applied hydraulic conditions. For tangential wave experiments, the A and B values were obtained as 51 mm/h and −0.1 mm/N from the numerical fitting. For the perpendicular wave experiment, the A and B values were obtained as 46.17 mm/h and −0.2 mm/N, indicating that the decline in average erosion rate with the increase in biocementation levels was more drastic in the case of perpendicular waves than the tangential waves.

3.4 Microstructure analysis

To illustrate the mechanism of grain binding, optical microscope images along with SEM micrographs of the samples treated with moderate (M4) and extreme levels (M8) of MICP are presented in Fig. 15. Untreated sand gains were observed with smooth surfaces, as illustrated in Fig. 15a and d. The clusters of rhombohedral CaCO$_3$ crystals (CC) were observed in the moderately biocemented sand over the smooth surface and grooves of the sand grains making the surface rough, as illustrated in Fig. 15b and e. The resulting interparticle locking of the sand grains is most likely the reason for the notable improvement in erosion resistance of the soil. The increased roughness leading to an improved interparticle locking of the grains has been reported to improve the shear strength of the soil [1, 9, 12]. For the extreme biocementation, residual samples from PM8 and TM8 were considered. The heavily biocemented sand grains were observed to be
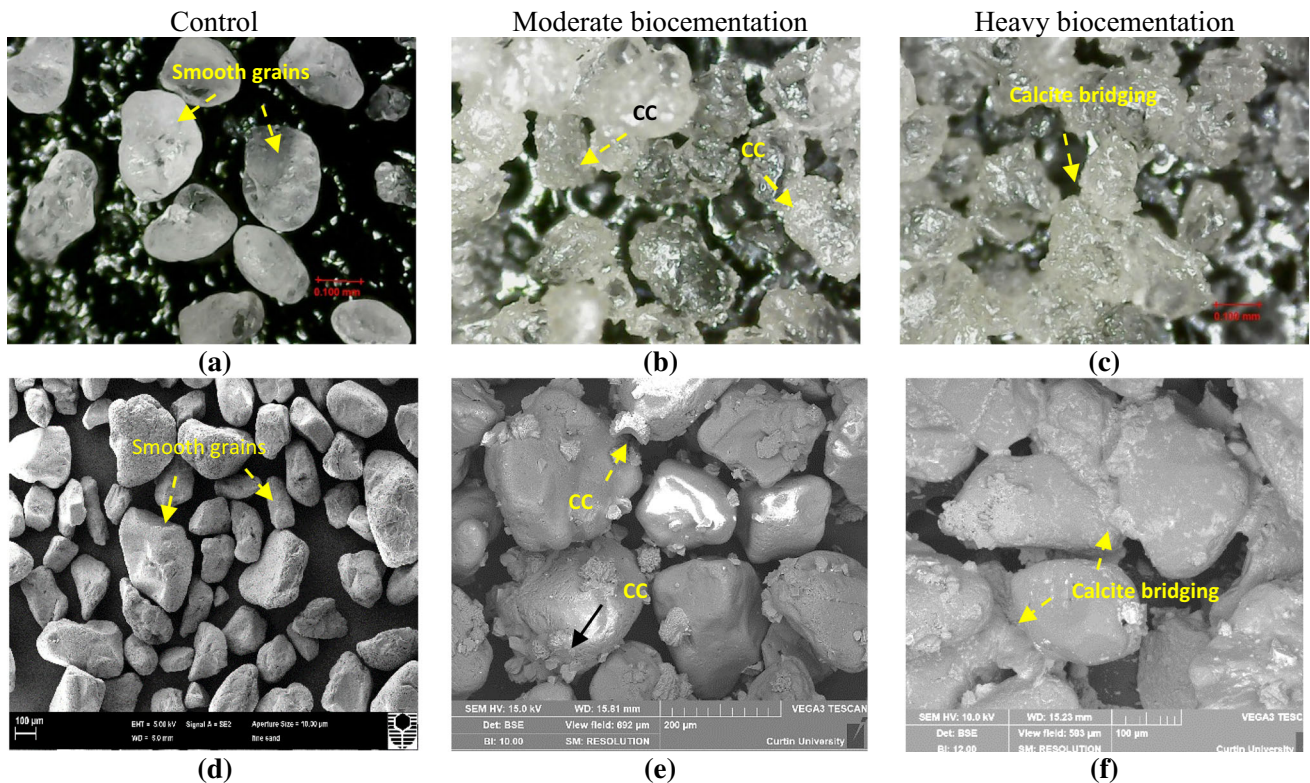

Fig. 14 Correlation of average erosion rate with needle penetration index (NPI)

Fig. 15 Optical and Scanning Electron Microscope images of **a**, **d** Untreated sand- M0; **b**, **e** Moderately biocemented specimens- M4; and **c**, **f** Heavily biocemented specimens-M8

covered and bridged with biocement, as illustrated in Fig. 15c and f. The substantial precipitation of $CaCO_3$ over sand grains has led to grain bridging and significant improvement of erosion resistance. However, at high wave energy, these samples fragmented into large chunks. Excessive precipitation around the $CaCO_3$ bridging is possibly the major contributor to the brittleness in the heavily biocemented samples.

In Fig. 16, the microscopic images of XM treated specimens are shown. Figure 16a and d represents the control samples PXM0 and TXM0, which are devoid of calcium carbonate crystals. The SEM image in Fig. 16 (d) demonstrates a thin biopolymer (Bp) bridging between two sand grains. In PXM2 and TXM2, the $CaCO_3$ crystals were detected along with the stretched threads of biopolymer (Bp) on sand grains, as shown in Fig. 16b and e. On the other hand, PXM4 and TXM4 were observed to be covered in biocement, as illustrated in Fig. 16c and f. The threads of the biopolymer were also observed in PXM4 and TXM4. With higher magnification images, the structure of the biopolymer-biocement crust was discovered. Figure 17 illustrates an SEM micrograph of the PXM4 samples. A thick cluster of rhombohedral precipitates anchoring on the biopolymer layer was observed, confirming that biopolymer assists in localising the

precipitation. Since biopolymers are known to improve the shear strength of soil maintaining the ductility [43], the composite of biopolymer and biocement lead to the unparalleled erosion resilience of TXM4 and PXM4, despite having lesser $CaCO_3$ content than the conventionally biocemented samples TM6/PM6 and TM8/PM8.

The mineralogical analysis with the XRD plots verified the presence of different polymorphs in the precipitated $CaCO_3$. The predominance of quartz (Q) was detected in the untreated sand. No peaks responding to $CaCO_3$ crystals were observed in the untreated sand. All the biocemented samples and bio-composite treated specimens exhibited peaks of calcite (C104), confirming the presence of calcite [63]. The plots of XRD were coinciding for all the samples. Therefore, plots corresponding to TM8 and TM0 is presented in Fig. 18. Smaller peaks of vaterite were also observed for samples TM6/PM6 and TM8/PM8.

Calcite, vaterite and aragonite are the three anhydrous polymorphs of $CaCO_3$, which could be precipitated with the MICP process [33, 50]. Calcite is the most stable polymorph of $CaCO_3$ that exhibits euhedral shapes, whereas vaterite is known to have a spheroid cauliflower-like shape. Aragonite is rarely reported in MICP and have morning star-like morphology [50]. Calcite bridging is reported to induce higher strength in soils than vaterite
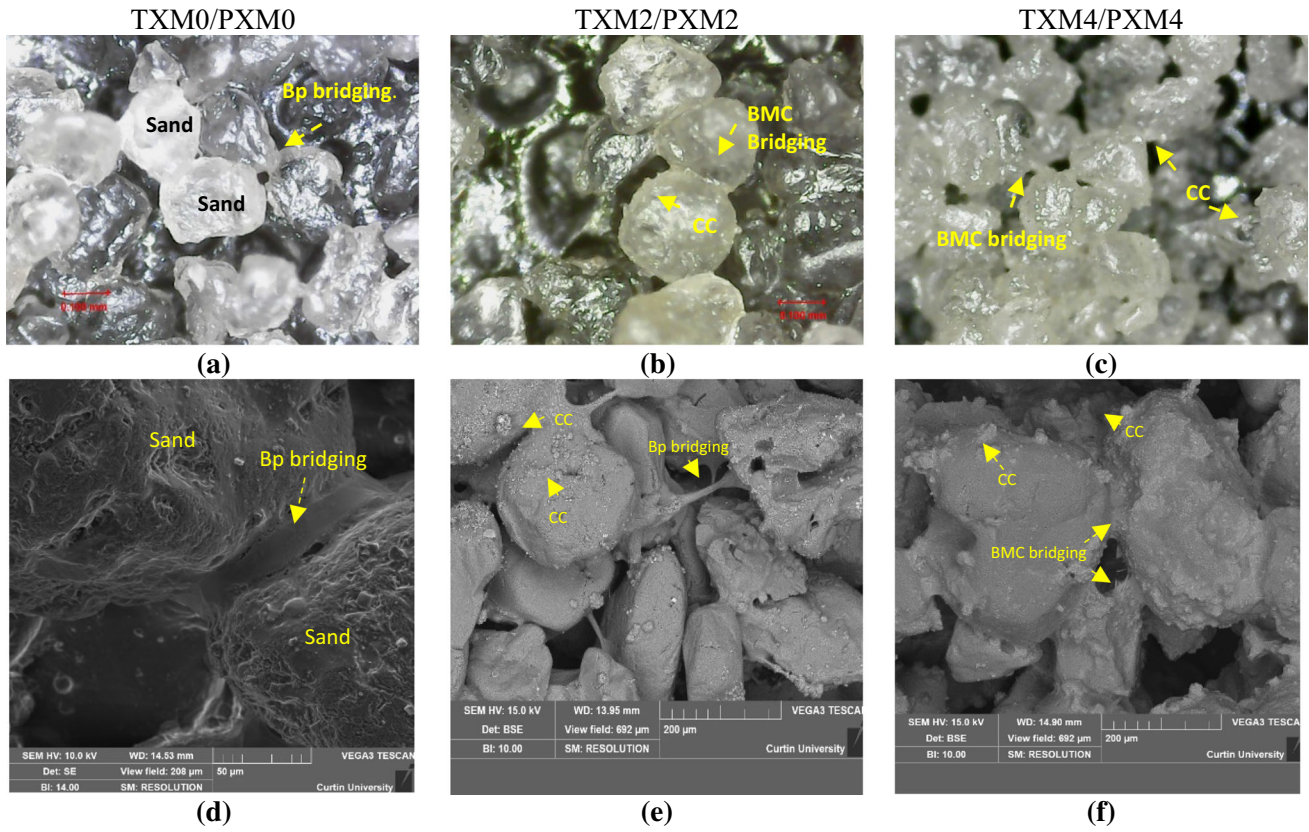
TXM0/PXM0 TXM2/PXM2 TXM4/PXM4

(a) **(b)** **(c)**

(d) **(e)** **(f)**

Fig. 16 Optical and Scanning Electron Microscope images of **a**, **d** Plain biopolymer treated sand- XM0; and Biopolymer-biocement composite treated specimen **b**, **e** XM2; and **c**, **f** XM4
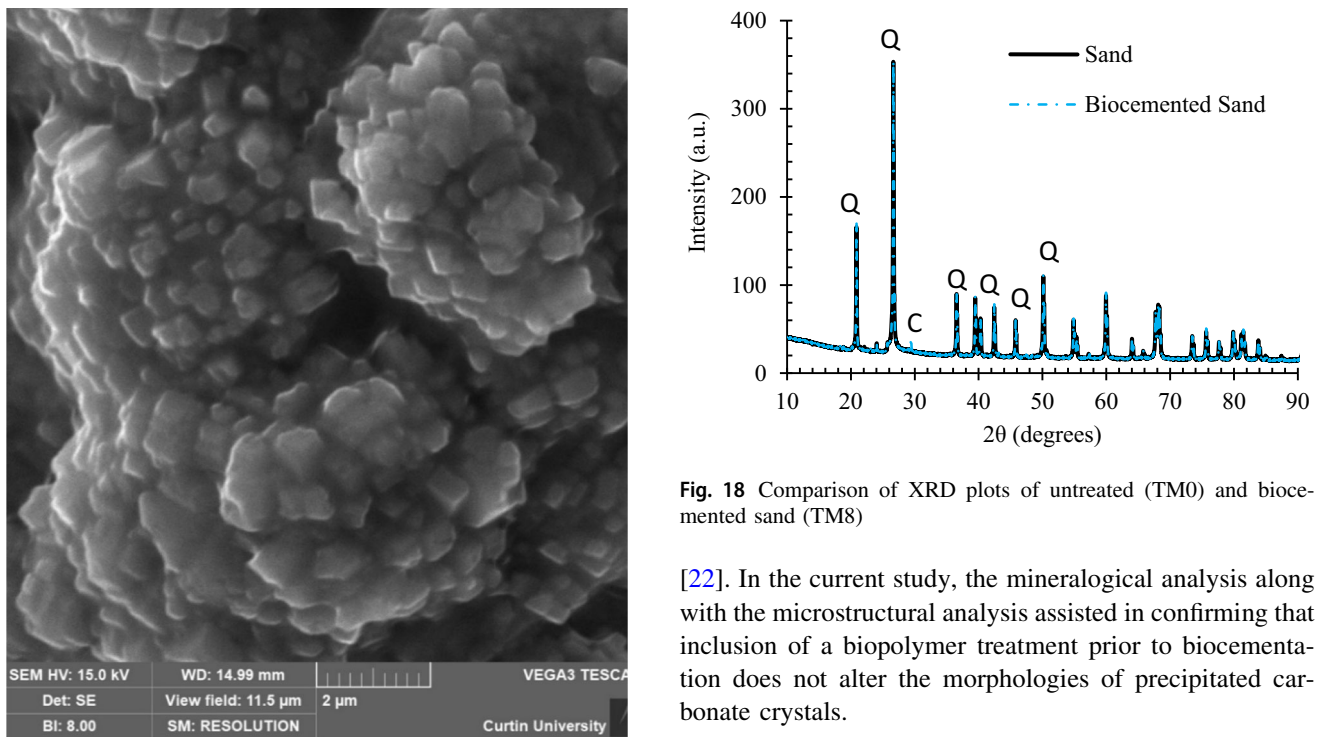

Fig. 17 Anchored $CaCO_3$ cluster in the BMC bridge (Sample XM4)

Fig. 18 Comparison of XRD plots of untreated (TM0) and biocemented sand (TM8)

[22]. In the current study, the mineralogical analysis along with the microstructural analysis assisted in confirming that inclusion of a biopolymer treatment prior to biocementation does not alter the morphologies of precipitated carbonate crystals.

3.5 Cost and construction-efficiency

DeJong et al., 2013 [16] reported that the cost of implementing conventional MICP for soil improvement to the field might vary from US$ $75/m^3$ to US$ $500/m^3$, which depends on the levels of biocementation, quality of cementation reagents, and cost of implementation including electricity, labour & transport. Ivanov and Chu, 2008 [36] reported that the material cost for conventional MICP can vary between from US$ $0.5/m^3$ to US$ $9/m^3$, while the conventional soil grouting materials such as acrylamide, polyurethane, phenoplast and sodium silicate costs are reported in a range of from US$ $2/m^3$ to US$ $72/m^3$. As per the current rates for industrial-grade biocementing reagents (> 95% purity), the costs for proposed strategies M8 and XM4 was estimated at around US$ $9/m^2$ and US$ $4.6/m^2$, respectively. The estimates are for a 5 cm target depth of biocemented crust. The cost can be reduced further by utilising commercially available low-cost biocementation reagents. The material costs for conventionally used temporary/flexible erosion control products (Aussie Environmental, Australia, Certified Professionals in Erosion and Sediment Control) are given in Table 2.

On the other hand, a report by the environmental agency, UK [35] described that the rigid concrete structures such as sea defences, retaining walls and sea walls may cost as high as 750 US$/$m^2$ to 7500 US$/$m^2$ (543 to 5467 £/m^2). The flexible erosion control systems do not exhibit strength characteristics, but it is the most used product due to their low cost, as mentioned in Table 2.

The proposed method in the current study aims to replace the soil grouting materials. The water-like permeability of the reagents and low-viscosity biopolymer solution allows the proposed method for a convenient field application by spraying strategy. Although the findings from the current study suggested that the proposed composite treatment could prevent wave erosion to a great extent, a metre-scale pilot study is necessary to determine its feasibility in terms of cost-effectiveness and construction efficiency. The $CaCO_3$ evolution with depth is a very

important parameter that derives the erosion resistance of the biocemented crust. In the current study, the $CaCO_3$ variation with depth was not addressed as the soil samples were small in size. Moreover, it is critical to evaluate the long-term performance of metre-scale biocemented soil against different types of waves for determining the design-period of the proposed treatment.

4 Conclusion

Soil erosion at beaches and riverbanks leads to enormous loss of infrastructure. The conservation of soil with natural aggregation processes has a significant potential for developing an ecologically conscious alternative to current practices. In the present study, various levels of biocementation are compared against perpendicular and tangential flowing hydraulic waves in a lab-scale flume. The potential of bio-composite treatment for improving the erosion resistance of the soil against the hydraulic waves is tested for the first time. The strength of the biocemented soil is evaluated with a non-destructive needle penetration test and is correlated with precipitated calcium carbonate content. The behaviour of the biocemented sand is also interpreted with its microstructure and mineralogy. The major findings from the present study are as follows:

1. In the case of perpendicular waves, the erosion declined consistently with the increase in biocementation levels. Within the investigated $CaCO_3$ precipitation range, the specimen with a calcite content around 98 mg/g-sand and NPI of 21 N/mm was found to be most effective to cease the soil erosion against imparted wave energy density of 6 J/cm^2 with the conventional biocementation approach.

2. In the case of tangential waves, the erosion decreased considerably with an increase in biocementation levels. However, the erosion did not completely cease. Even with a high calcite content of around 92.5 mg/g-sand and NPI value around 21 N/mm, the biocemented sand eroded more than 40% of its initial volume at a wave energy density of 5.3 J/cm^2.

3. The composite with biopolymer aided biocement had lower erosion compared to conventional biocement against both perpendicular and tangential waves. A sample with 56.5 mg/g-sand and NPI of 10.7 N/mm was observed to bring down the eroded volume to 20% against the tangential hydraulic wave of energy density 5.3 J/cm^2.

4. The collaborative influence of biopolymer-biocement composites was analysed with the microstructure analysis. Clusters of rhombohedral calcite crystals

Table 2 Comparison of costs of existing erosion control products

Products	Market price/ unit (US$)	Dimension (m × m)	Cost (US$/$m^2$)
Filled sandbags (Poly-woven)	5.95	0.42 × 0.3	34
Jute textile	142	1.8 × 25	3.15
Coir mesh brick (700 GSM)	115	2 × 25	2.3
Geofabric (140 GSM)	95	2 × 50	0.95

were observed to be anchored in the biopolymer layer, which provided enhanced efficiency against erosion.

5. The biopolymer-biocement composite required only four cycles of biocementation (XM4) to produce the most efficient erosion resistance, which turns out to be only 50% of cementation reagents in comparison to sole biocementation treatment with MICP (M8). Hence, the biopolymer aided biocemented samples will result in 50% material savings, and therefore, it would stoichiometrically produce 50% lesser ammonia. However, the generated ammonia was not measured in the current study, and therefore, future studies with real-time monitoring of generated ammonia are recommended.

While the findings from the current study provide several useful insights about the erosion characteristics of biocemented and biopolymer-biocement composite treated sand against two different kinds of waves, numerous important factors such as type of soils, different mixtures of biopolymer, and concentrations of cementation solution were neglected to make the study succinct. These factors may influence the suggested recommendations. Further research using different types of biopolymers, soils and slope angles are advised with real-time monitoring of biogeochemical reactions for the optimisation of treatment protocols. Even with the above-mentioned constraints, the study demonstrates that the biocementation technique might not be a panacea against wave-induced soil erosion, specifically against the tangential flow. Although there are several challenges in the application of proposed technology for ecologically sensitive coastal and riverbank zones (including the quantity of generated ammonia and the brittle nature of biocemented soil), many of the factors can be tackled up to a certain extent with the proposed bio-composite treatment.

Authors' contributions AAD and JHL contributed to fieldwork, experiments, analysis of data. NKD designed the biological experiments and sample treatment procedure. KR and AM contributed to the conceptualisation and supervision of the experiments. The first draft was prepared and revised by AAD and AM. All authors have approved the final version of the manuscript.

Declarations

Conflict of interest The authors declare that they have no conflict of interest.

References

1. Al Qabany A, Soga K (2013) Effect of chemical treatment used in MICP on engineering properties of cemented soils. Géotechnique 63:331–339. https://doi.org/10.1680/geot.SIP13.P.022
2. Ashton A, Murray AB, Arnoult O (2002) Formation of coastline features by large-scale instabilities induced by high-angle waves. Nature 415:666–666. https://doi.org/10.1038/415666a
3. ASTM D4254-16 (2006) Standard Test Methods for Minimum Index Density and Unit Weight of Soils and Calculation of Relative Density. ASTM Int. West Conshohocken, PA.
4. ASTM D4972-19 (2019) Standard Test Methods for pH of Soils. ASTM Int. West Conshohocken, PA.
5. ASTM D6913/D6913M-17 (2017) Standard Test methods for Particle-Size Distribution (Gradation) of Soils Using Sieve Analysis. ASTM Int. West Conshohocken, PA.
6. ASTM D854-14 (2014) Standard Test Methods for Specific Gravity of Soil Solids by Water Pycnometer. ASTM Int. West Conshohocken, PA.
7. Behzadipour H, Sadrekarimi A (2021) Biochar-assisted bio-cementation of a sand using native bacteria. Bull Eng Geol Environ. https://doi.org/10.1007/s10064-021-02235-0
8. Briaud J-L (2008) Case Histories in soil and rock erosion: woodrow wilson bridge, brazos river Meander, Normandy Cliffs, and New Orleans Levees. J Geotech Geoenvironmental Eng 134:1425–1447. https://doi.org/10.1061/(ASCE)1090-0241(2008)134:10(1425)
9. Cheng L, Cord-Ruwisch R, Shahin M (2013) Cementation of sand soil by microbially induced calcite precipitation at various degrees of saturation. Can Geotech J 50:81–90. https://doi.org/10.1139/cgj-2012-0023
10. Choi S-G, Park S-S, Wu S, Chu J (2017) Methods for calcium carbonate content measurement of biocemented soils. J Mater Civ Eng 29:1–4. https://doi.org/10.1061/(ASCE)
11. Chu J, Ivanov V, Naeimi M et al (2014) Optimization of calcium-based bioclogging and biocementation of sand. Acta Geotech 9:277–285. https://doi.org/10.1007/s11440-013-0278-8

12. Chung H, Kim SH, Nam K (2021) Application of microbially induced calcite precipitation to prevent soil loss by rainfall: effect of particle size and organic matter content. J Soils Sediments. https://doi.org/10.1007/s11368-020-02757-2

13. Clarà Saracho A, Haigh SK, Ehsan Jorat M (2021) Flume study on the effects of microbial induced calcium carbonate precipitation (MICP) on the erosional behaviour of fine sand. Géotechnique. https://doi.org/10.1680/jgeot.19.P.350

14. Das VK, Roy S, Barman K et al (2020) Cohesive river bank erosion mechanism under wave-current interaction: a flume study. J Earth Syst Sci 129:99. https://doi.org/10.1007/s12040-020-1363-7

15. DeJong JT, Mortensen BM, Martinez BC, Nelson DC (2010) Bio-mediated soil improvement. Ecol Eng 36:197–210. https://doi.org/10.1016/j.ecoleng.2008.12.029

16. DeJong JT, Soga K, Kavazanjian E et al (2013) Biogeochemical processes and geotechnical applications: progress, opportunities and challenges. Géotechnique 63:287–301. https://doi.org/10.1680/geot.SIP13.P.017

17. Devrani R, Dubey AA, Ravi K, Sahoo L (2021) Applications of bio-cementation and bio-polymerization for aeolian erosion control. J Arid Environ 187:104433. https://doi.org/10.1016/j.jaridenv.2020.104433

18. Dhami NK, Alsubhi WR, Watkin E, Mukherjee A (2017) Bacterial community dynamics and biocement formation during stimulation and augmentation: implications for soil consolidation. Front Microbiol. https://doi.org/10.3389/fmicb.2017.01267

19. Dhami NK, Reddy MS, Mukherjee A (2013) Biomineralization of calcium carbonates and their engineered applications: a review. Front Microbiol 4:1–13. https://doi.org/10.3389/fmicb.2013.00314

20. Dipova N (2018) Nondestructive testing of stabilized soils and soft rocks via needle penetration. Period Polytech Civ Eng. https://doi.org/10.3311/PPci.11874

21. Do J, Montoya BM, Gabr MA (2021) Scour mitigation and erodibility improvement using microbially induced carbonate precipitation. Geotech Test J. https://doi.org/10.1520/GTJ20190478

22. Dubey AA, Murugan R, Ravi K et al (2022) Investigation on the impact of cementation media concentration on properties of biocement under stimulation and augmentation approaches. J Hazard Toxic Radioact Waste 26:1–13. https://doi.org/10.1061/(ASCE)HZ.2153-5515.0000662

23. Dubey AA, Devrani R, Ravi K et al (2021) Experimental investigation to mitigate aeolian erosion via biocementation employed with a novel ureolytic soil isolate. Aeolian Res 52:100727. https://doi.org/10.1016/j.aeolia.2021.100727

24. Dubey AA, Dhami NK, Mukherjee A et al (2021) Investigating the potential of xanthan gum for aeolian erosion mitigation. In: Sitharam TG, Parthasarathy CR, Kolathayar S (eds) Ground improvement techniques, vol 118. Springer, Singapore, pp 379–386

25. Dubey AA, Ravi K, Mukherjee A et al (2021) Biocementation mediated by native microbes from Brahmaputra riverbank for mitigation of soil erodibility. Sci Rep 11:15250. https://doi.org/10.1038/s41598-021-94614-6

26. Dubey AA, Ravi K, Shahin MA et al (2021) Bio-composites treatment for mitigation of current-induced riverbank soil erosion. Sci Total Environ 800:149513. https://doi.org/10.1016/j.scitotenv.2021.149513

27. Faure YH, Ho CC, Chen RH et al (2010) A wave flume experiment for studying erosion mechanism of revetments using geotextiles. Geotext Geomembr 28:360–373. https://doi.org/10.1016/j.geotexmem.2009.11.002

28. Feng K, Montoya BM (2016) Influence of confinement and cementation level on the behavior of microbial-induced calcite precipitated Sands under monotonic drained loading. J Geotech Geoenviron Eng 2:04015057. https://doi.org/10.1061/(ASCE)GT.1943-5606.0001379

29. Flemming BW (2011) Geology, morphology, and sedimentology of estuaries and coasts. In: Flemming BW, Hansom JD (eds) Treatise on estuarine and coastal science. Elsevier, Amsterdam, pp 7–38

30. Fujita Y, Taylor JL, Wendt LM et al (2010) Evaluating the potential of native ureolytic microbes to remediate a 90Sr contaminated environment. Environ Sci Technol 44:7652–7658. https://doi.org/10.1021/es101752p

31. Gomez MG, Graddy CMR, DeJong JT, Nelson DC (2019) Biogeochemical changes during bio-cementation mediated by stimulated and augmented ureolytic microorganisms. Sci Rep 9:1–15. https://doi.org/10.1038/s41598-019-47973-0

32. Gu J, Liu G, Elbasit A, Mohamed MA, Shi HQ (2020) Response of slope surface roughness to wave-induced erosion during water level fluctuating. J Mt Sci 17(4):871–883. https://doi.org/10.1007/s11629-019-5745-8

33. Hammes F, Boon N, De Villiers J et al (2003) Strain-specific ureolytic microbial calcium carbonate precipitation. Appl Environ Microbiol 69:4901–4909. https://doi.org/10.1128/AEM.69.8.4901-4909.2003

34. Harkes MP, van Paassen LA, Booster JL et al (2010) Fixation and distribution of bacterial activity in sand to induce carbonate precipitation for ground reinforcement. Ecol Eng 36:112–117. https://doi.org/10.1016/j.ecoleng.2009.01.004

35. Hudson T, Keating K, Petit A (2015) Cost estimation for coastal protection—summary of evidence. Environ Agency, Horiz House, Deanery Road, Bristol, BS1 5AH 37

36. Ivanov V, Chu J (2008) Applications of microorganisms to geotechnical engineering for bioclogging and biocementation of soil in situ. Rev Environ Sci Bio/Technol 7:139–153. https://doi.org/10.1007/s11157-007-9126-3

37. Jiang C, Wu Z, Chen J et al (2017) An available formula of the sandy beach state induced by plunging waves. Acta Oceanol Sin 36:91–100. https://doi.org/10.1007/s13131-017-1114-z

38. Jiang N-J, Soga K (2017) The applicability of microbially induced calcite precipitation (MICP) for internal erosion control in gravel–sand mixtures. Géotechnique 67:42–55. https://doi.org/10.1680/jgeot.15.P.182

39. Jiang NJ, Tang CS, Yin LY et al (2019) Applicability of microbial calcification method for sandy-slope surface erosion control. J Mater Civ Eng 31:1–11. https://doi.org/10.1061/(ASCE)MT.1943-5533.0002897

40. Karol RH (2003) Chemical grouting and soil stabilization, 3rd edn. Marcel Dekker, New York

41. Kou H, Wu C, Ni P, Jang B (2020) Assessment of erosion resistance of biocemented sandy slope subjected to wave actions. Appl Ocean Res 105:102401. https://doi.org/10.1016/j.apor.2020.102401

42. Lai HJ, Cui MJ, Wu SF et al (2021) Retarding effect of concentration of cementation solution on biocementation of soil. Acta Geotech 16:1457–1472. https://doi.org/10.1007/s11440-021-01149-1

43. Lee S, Chung M, Park HM et al (2019) Xanthan gum biopolymer as soil-stabilization binder for road construction using local soil in Sri Lanka. J Mater Civ Eng 31:06019012. https://doi.org/10.1061/(ASCE)MT.1943-5533.0002909

44. Liu K-W, Jiang N-J, Qin J-D et al (2021) An experimental study of mitigating coastal sand dune erosion by microbial- and enzymatic-induced carbonate precipitation. Acta Geotech 16:467–480. https://doi.org/10.1007/s11440-020-01046-z

45. Mujah D, Cheng L, Shahin MA (2019) Microstructural and geomechanical study on biocemented sand for optimization of

micp process. J Mater Civ Eng 31:04019025. https://doi.org/10.1061/(ASCE)MT.1943-5533.0002660

46. Mujah D, Shahin MA, Cheng L (2017) State-of-the-art review of biocementation by microbially induced calcite precipitation (MICP) for soil stabilization. Geomicrobiol J 34:524–537. https://doi.org/10.1080/01490451.2016.1225866

47. Murugan R, Suraishkumar GK, Mukherjee A, Dhami NK (2021) Insights into the influence of cell concentration in design and development of microbially induced calcium carbonate precipitation (MICP) process. PLoS ONE 16(7):e0254536. https://doi.org/10.1371/journal.pone.0254536

48. Ramachandran AL, Dubey AA, Dhami NK, Mukherjee A (2021) Multiscale study of soil stabilization using bacterial biopolymers. J Geotech Geoenvironmental Eng 147:04021074. https://doi.org/10.1061/(ASCE)GT.1943-5606.0002575

49. Ramachandran AL, Polat P, Mukherjee A, Dhami NK (2020) Understanding and creating biocementing beachrocks via biostimulation of indigenous microbial communities. Appl Microbiol Biotechnol 104:3655–3673. https://doi.org/10.1007/s00253-020-10474-6

50. Rodriguez-Navarro C, Jroundi F, Schiro M et al (2012) Influence of substrate mineralogy on bacterial mineralization of calcium carbonate: implications for stone conservation. Appl Environ Microbiol 78:4017–4029. https://doi.org/10.1128/AEM.07044-11

51. Salifu E, MacLachlan E, Iyer KR et al (2016) Application of microbially induced calcite precipitation in erosion mitigation and stabilisation of sandy soil foreshore slopes: a preliminary investigation. Eng Geol 201:96–105. https://doi.org/10.1016/j.enggeo.2015.12.027

52. Scheres B, Schüttrumpf H (2020) Investigating the erosion resistance of different vegetated surfaces for ecological enhancement of Sea Dikes. J Mar Sci Eng 8:519. https://doi.org/10.3390/jmse8070519

53. Shahin MA, Jamieson K, Cheng L (2020) Microbial-induced carbonate precipitation for coastal erosion mitigation of sandy slopes. Géotech Lett 10:1–5. https://doi.org/10.1680/jgele.19.00093

54. Sharma M, Satyam N, Reddy KR (2020) Strength enhancement and lead immobilization of sand using consortia of bacteria and blue-green Algae. J Hazard Toxic Radioact Waste 24:04020049. https://doi.org/10.1061/(ASCE)HZ.2153-5515.0000548

55. Skafel MG, Bishop CT (1994) Flume experiments on the erosion of till shores by waves. Coast Eng 23:329–348. https://doi.org/10.1016/0378-3839(94)90009-4

56. Fredsøe J, Deigaard R (1992) Mechanics of coastal sediment transport. World Sci. https://doi.org/10.1142/1546

57. Terzis D, Laloui L (2019) A decade of progress and turning points in the understanding of bio-improved soils: a review. Geomech Energy Environ 19:100116. https://doi.org/10.1016/j.gete.2019.03.001

58. Ulusay R, Aydan Ö, Erguler ZA et al (2014) ISRM suggested method for the needle penetration test. Rock Mech Rock Eng 47:1073–1085. https://doi.org/10.1007/s00603-013-0534-0

59. Ulusay R, Erguler ZA (2012) Needle penetration test: Evaluation of its performance and possible uses in predicting strength of weak and soft rocks. Eng Geol 149–150:47–56. https://doi.org/10.1016/j.enggeo.2012.08.007

60. United States Environmental Protection Agency (2017) National management measures to control nonpoint source pollution from hydromodification. Washington, DC

61. van Rijn LC, Walstra D-JR, van Ormondt M (2007) Unified view of sediment transport by currents and waves. IV: application of morphodynamic model. J Hydraul Eng 133:776–793. https://doi.org/10.1061/(ASCE)0733-9429(2007)133:7(776)

62. Wang X, Tao J, Bao R et al (2018) Surficial soil stabilization against water-induced erosion using polymer-modified microbially induced carbonate precipitation. J Mater Civ Eng 30:04018267. https://doi.org/10.1061/(ASCE)MT.1943-5533.0002490

63. Wen K, Li Y, Amini F, Li L (2020) Impact of bacteria and urease concentration on precipitation kinetics and crystal morphology of calcium carbonate. Acta Geotech 15:17–27. https://doi.org/10.1007/s11440-019-00899-3

64. Whiffin VS (2004) Microbial CaCO$_3$ Precipitation for the PRODUCTION OF BIOCEMENT. Doctoral Thesis, Murdoch University, Western Australia.

65. Yang J, Pan X, Zhao C et al (2016) Bioimmobilization of heavy metals in acidic copper mine tailings soil. Geomicrobiol J 33:261–266. https://doi.org/10.1080/01490451.2015.1068889

66. Zhang M, Lu Z, Bai Q et al (2020) Effect of microsprinkler irrigation under plastic film on photosynthesis and fruit yield of greenhouse tomato. J Sensors. https://doi.org/10.1155/2020/8849419

67. Zuazo VHD, Pleguezuelo CRR (2008) Soil-erosion and runoff prevention by plant covers: a review Agron. Sustain Dev 8:65–86. https://doi.org/10.1051/agro:2007062